RESEARCH ARTICLE

Fabrication and characterization of magnetically responsive Fe$_3$O$_4$@TiO$_2$ core-shell adsorbent for enhanced thallium removal

Zhihan Yang[1] · Wanlin Wu[1] · Ling Yu[2] · Xiaoyun Fan[1] · Yang Yu[1]

Abstract

Thallium (Tl) contamination in natural waters can pose a severe risk to human health. In this study, a magnetically responsive Fe$_3$O$_4$@TiO$_2$ core-shell adsorbent was developed for the effective removal of thallium(I) from water. The isoelectric point of the adsorbent surface was decreased from 6.0 to 4.8 due to the loading of nano-sized TiO$_2$, leading to an enhanced electrostatic interaction between the adsorbent and Tl(I) ions in a wider pH range. The Fe$_3$O$_4$@TiO$_2$ magnetic adsorbent exhibited a threefold higher BET specific surface area compared to pristine Fe$_3$O$_4$ particles. The kinetics study showed that approximately 82% of the maximum Tl(I) loading amount could be achieved within 30 min at the initial Tl(I) concentration of 8 mg/L and adsorbent dosage of 0.1 g/L. The adsorption of Tl(I) was significantly increased with increasing solution pH. The experimental data was better fitted by the Langmuir and Temkin isotherms than the Freundlich isotherm and the maximum adsorption capacity of the magnetic adsorbent was 101.5 mg/g at pH 7.0. The interference of co-existing cations in the Tl(I) adsorption followed the subsequence: Cu^{2+} > Mg^{2+} > Ca^{2+} > Na$^+$. The hydroxyl groups bonded on titanium atoms might play a key role in the uptake of Tl(I) ions. During the adsorption, the Tl(I) ions can be effectively adsorbed on the adsorbent surface via the formation of Ti–O–Tl linkages.

Keywords Adsorption · Thallium · Magnetic adsorbent · Titanium oxide · Mechanism

Introduction

Thallium (Tl) as a toxic heavy metal element can originate from both natural processes and anthropogenic activities. Long-term exposure to thallium even under its low concentration can cause a variety of health problems such as hair loss; abdominal pain; anorexia; ataxia; paresthesia; pathologic changes in the kidney,

liver, and lung; cancers; and death (Galván-Arzate 1998; Mulkey and Oehme 1993). The maximum contaminant level (MCL) of thallium in drinking water is therefore limited to 2 μg/L by the US Environmental Protection Agency (USEPA).

Technologies such as ion exchange (Li et al. 2017), coagulation oxidation (Zhang et al. 2013), chemical precipitation (Davies et al. 2016), emulsion liquid membrane (Yang et al. 2017), and adsorption (Liu et al. 2014; Memon et al. 2008; Zhang et al. 2018) have been applied for the removal of thallium from water. Among them, adsorption process is considered as one of the most promising methods due to its high efficiency, low cost, feasibility, and availability of numerous adsorbents including activated carbon (Sabermahani et al. 2017), multiwalled carbon nanotube (Pu et al. 2013; Rehman et al. 2013), biomass wastes (Khavidaki and Aghaie 2013; Memon et al. 2008; Peter and Viraraghavan 2008), and metal oxides (Huangfu et al. 2015; Kajitvichyanukul et al. 2003; Wan et al. 2014; Zhang et al. 2008). The abovementioned adsorbents mainly suffer from the difficulty in separation from the treated stream, and centrifuge or filtration with high energy consumption is therefore generally required as the post-treatment approach (Yin et al. 2017).

Highlights • Fe$_3$O$_4$@TiO$_2$ core-shell adsorbent was prepared for the removal of Tl(I).
• Eighty-two percent of equilibrium adsorption capacity can be obtained in the first 30 min.
• TiO$_2$ on the adsorbent surface was responsible for the effective removal of Tl(I).
• Tl(I) was adsorbed on the adsorbent surface via the formation of Ti–O–Tl linkages.

✉ Yang Yu
yuyang@jnu.edu.cn

[1] Guangdong Key Laboratory of Environmental Pollution and Health, School of Environment, Jinan University, Guangzhou 511443, China

[2] Analysis and Test Center, Guangdong University of Technology, Guangzhou 510006, China

Magnetic adsorbents would be a better choice for the practical application because of their facile recovery with the assistance of external magnetic field (Lingamdinne et al. 2019; Ruthiraan et al. 2019). In order to obtain high-performance magnetic adsorbents, adsorptive materials with the special affinity towards target contaminants have been incorporated into magnetic support materials. The chitosan-coated Fe_3O_4 particles exhibited a rapid and efficient adsorption of Pb(II) ions from water (Rasoulzadeh et al. 2020). The adsorption ability of Fe_3O_4 particles was also demonstrated to be greatly improved by doping other metal oxides (Yu et al. 2018). Although this strategy is simple to handle, the crystal structure of Fe_3O_4 particles might be disturbed resulting in a negative effect on the magnetic separation performance. In comparison, the magnetic adsorbent with a core-shell structure can overcome drawbacks of the doping method. Moreover, the active sites from adsorptive materials will be fully exposed on the external surface of the magnetic adsorbent in which much faster adsorption rate can be expected. Up to now, numerous magnetic adsorbents have been developed for removing toxic pollutants, e.g., arsenic, lead, copper, mercury, and organic dyes (Alijani et al. 2015; Koduru et al. 2019; Lingamdinne et al. 2018). However, few studies on the removal of thallium using the magnetic adsorbent have been reported in the literature.

In this study, the $Fe_3O_4@TiO_2$ core-shell magnetic adsorbent was prepared by a simple co-precipitation method. The characteristics of the adsorbent including the surface morphology, particle size distribution, zeta potential, and crystal structure were studied. A series of batch experiments were conducted to investigate the adsorption performance of the adsorbent for the Tl(I) removal. The adsorption mechanism was also proposed according to the results of batch experiments and the X-ray photoelectron spectroscopy (XPS) analysis.

Materials and methods

Materials

Analytical-grade chemical reagents were used in this study, including iron(III) nitrate nonahydrate ($Fe(NO_3)_3 \cdot 9H_2O$), iron(II) sulfate heptahydrate ($FeSO_4 \cdot 7H_2O$), titanium butoxide ($C_{16}H_{36}O_4Ti$), sodium hydroxide (NaOH), nitric acid (HNO_3), thallium(I) nitrate ($TiNO_3$), sodium chloride (NaCl), magnesium chloride hexahydrate ($MgCl_2 \cdot 6H_2O$), calcium chloride dihydrate ($CaCl_2 \cdot 2H_2O$), and copper chloride dihydrate ($CuCl_2 \cdot 2H_2O$), which were purchased from Sigma-Aldrich. The Tl(I) stock solution with the concentration of 200 mg/L was prepared by dissolving $TiNO_3$ into deionized (DI) water. Working solutions were prepared by diluting the Tl(I) stock solution to predetermined concentrations with DI water.

Preparation of $Fe_3O_4@TiO_2$ core-shell magnetic adsorbent

The pristine magnetic particle (Fe_3O_4) was prepared by co-precipitation method. In brief, a certain amount of $Fe(NO_3)_3 \cdot 9H_2O$ and $FeSO_4 \cdot 7H_2O$ with the molar ratio of 2:1 was freshly dissolved into deoxygenated DI water and mechanically stirred under a nitrogen atmosphere at 80 °C. After that, NaOH solution was added dropwise into the mixture solution. The formed precipitates were collected, washed by DI water, and dried in oven at 60 °C.

Fifty milligrams of Fe_3O_4 powders were uniformly dispersed into 35-mL ethanol under ultrasonication. Two-milliliter titanium butoxide was then added under mechanical agitation to form a homogenous mixture. After that, 1:5 (V/V) DI/ethanol solution was added dropwise under stirring within 1 h. The obtained particles were magnetically separated using a permanent magnet and washed by DI/ethanol for several times. The samples were dried overnight at 60 °C. The TiO_2 particles were synthesized through the same procedure without adding Fe_3O_4 powders. The obtained white precipitates were collected using centrifuge, washed by DI/ethanol, and dried in oven for the later characterization.

Characterization

The surface morphology of TiO_2, Fe_3O_4, and $Fe_3O_4@TiO_2$ core-shell magnetic adsorbent was observed by a scanning electron microscopy (SEM, ZEISS EVO18, Germany). The crystal structure of the adsorbent was measured using X-ray diffraction (XRD, Bruker D2 Phaser, Germany) with Cu Kα radiation at 30 kV and 30 mA. The zeta potential and particle size distribution of TiO_2, Fe_3O_4, and $Fe_3O_4@TiO_2$ core-shell magnetic adsorbent were determined using dynamic light scattering (Zetasize nano ZSE, Malvern, UK). The solution pH at which the zeta potential equals zero is defined as the isoelectric point (IEP), which is widely used as an index of the equilibrium of protonation and deprotonation of functional groups on the adsorbent surface. At the pH value of IEP, the adsorbent surface would be neutrally charged. BET specific surface area and pore size distribution of Fe_3O_4 and $Fe_3O_4@TiO_2$ magnetic adsorbent were determined by the nitrogen adsorption isotherm technique using a Quantachrome Instruments analyzer (USA). The chemical state of surface elements and composition of oxygen-containing groups on virgin and Tl-loaded adsorbents were analyzed by XPS (Kratos XPS system-Axis His-165 Ultra, Shimadzu, Japan).

Batch experiments

All adsorption experiments were conducted at room temperature ($T = 25 \pm 1$ °C) and solution pH was maintained at the predetermined value throughout the adsorption process by
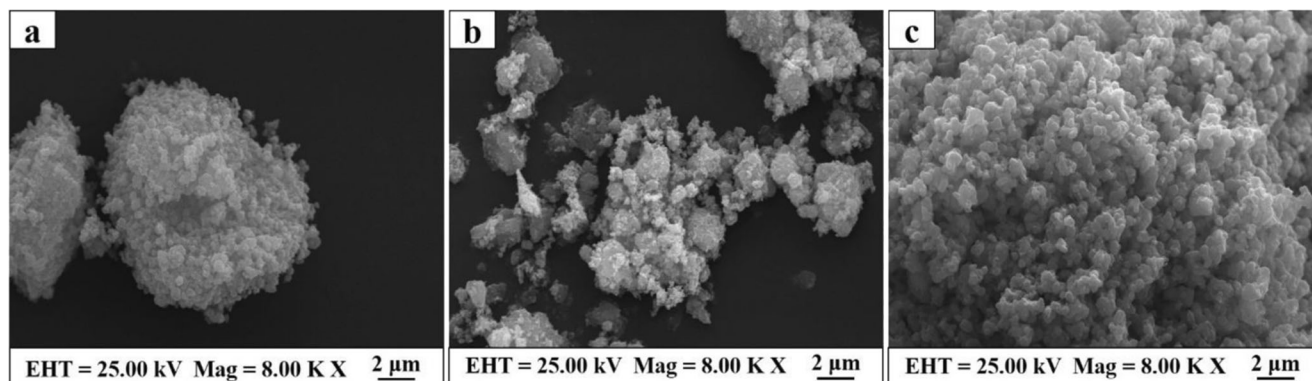
Fig. 1 SEM images of TiO$_2$ (**a**), Fe$_3$O$_4$ (**b**), and Fe$_3$O$_4$@TiO$_2$ magnetic adsorbent (**c**)

adding HNO$_3$ or NaOH. The Tl(I) concentration in solutions was measured using an inductively coupled plasma mass spectrometry (ICP-MS). The loading amount of Tl(I) on the adsorbent was calculated as below:

$$q_t = \frac{(C_0 - C_t)V}{m} \tag{1}$$

$$q_e = \frac{(C_0 - C_e)V}{m} \tag{2}$$

where q_t and q_e are the loading amount of Tl(I) on the adsorbent at time t and at equilibrium (mg/g), respectively; C_0, C_t, and C_e are the Tl(I) concentration at initial, at time t, and at equilibrium (mg/L), respectively; V is the volume of Tl(I) solution (L); m is the mass of the adsorbent (g).

In the experiment of adsorption kinetics, 0.1 g of adsorbent was added into 1-L Tl(I) solution with the initial Tl(I) concentration of 8 mg/L and solution pH was maintained at 7.0. Approximately 5-mL samples were taken at different time intervals and filtered through 0.45-μm cellulose membrane for the Tl(I) concentration measurement.

In the experiment of pH effect, a series of 100-mL Tl(I) solutions with the Tl(I) concentration of 8 mg/L were prepared in glass vials. Solution pH was respectively adjusted to the different values ranging from 3.0 to 10.0. The adsorbent dosage was 0.1 g/L. After mechanically shaken for 24 h, samples were taken and filtered for the concentration measurement. The concentration of titanium (Ti) and iron (Fe) in solutions after the adsorption was also determined to evaluate the stability of the adsorbent under different solution pH.

In the adsorption isotherm experiment, 100-mL Tl(I) solutions with the different initial Tl(I) concentrations ranging from 5 to 150 mg/L were prepared and the solution pH was controlled at 7.0. After adding 10 mg of adsorbent into each vial, the suspension was agitated for 24 h. At the end of the experiment, samples were taken and filtered for the analysis of residual Tl(I) concentration.

In order to investigate the influence of co-existing cations on the Tl(I) uptake, a certain amount of Na$^+$, Mg^{2+}, Ca^{2+}, and Cu^{2+} was respectively added into Tl(I) solutions with the initial Tl(I) concentration of 8 mg/L. Solution pH was controlled
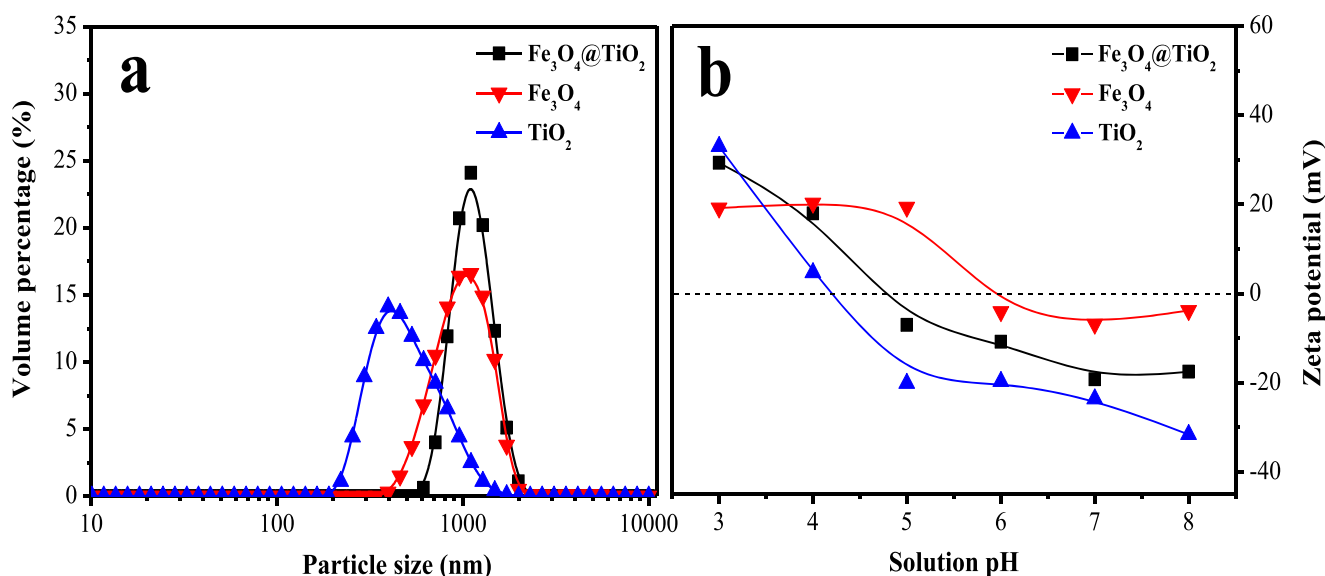
Fig. 2 Particle size distribution (**a**) and zeta potential (**b**) of Fe$_3$O$_4$@TiO$_2$ magnetic adsorbent, Fe$_3$O$_4$ and TiO$_2$

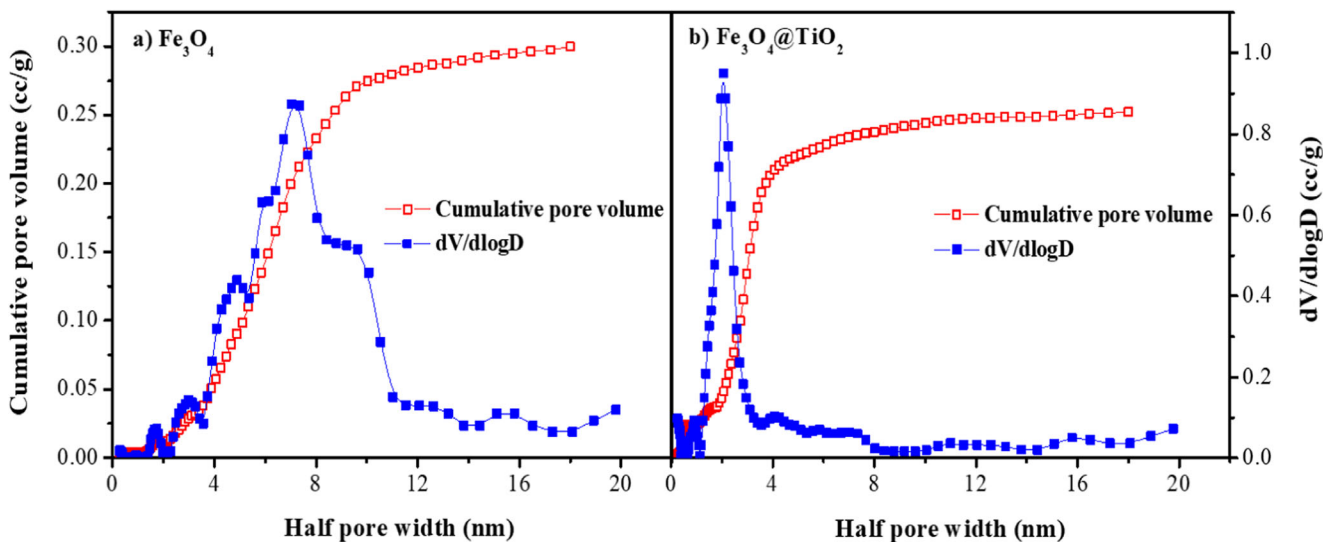**Fig. 3** XRD pattern of Fe$_3$O$_4$@TiO$_2$ magnetic adsorbent
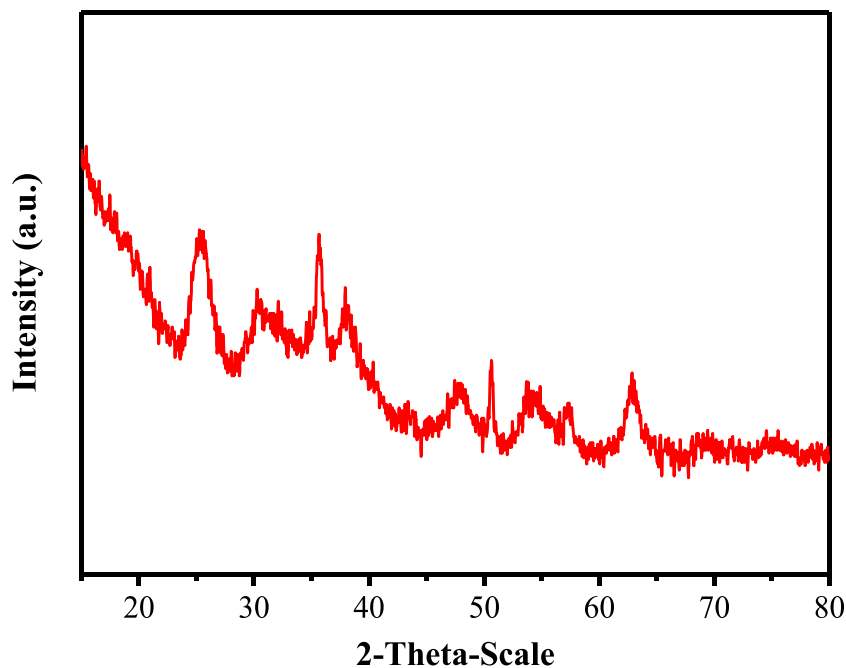
at 5.0 during the experiment to avoid the precipitation of cations. The adsorbent dosage was 0.1 g/L. After reaction for 24 h, samples were taken for the concentration measurement.

The regeneration performance of the adsorbent was evaluated through three-cycle adsorption and desorption experiments. 0.1 g of the virgin adsorbent was added into 1-L Tl(I) solution with the concentration of 8 mg/L under stirring and solution pH was controlled at 7.0. The spent adsorbent was collected using centrifuge after the adsorption and regenerated by 0.1 M HNO$_3$ solution for 3 h. The regenerated adsorbent was washed by DI water and then used for the next cycle of adsorption experiment.

Results and discussion

Characterization of adsorbents

The surface morphology of TiO$_2$, Fe$_3$O$_4$, and Fe$_3$O$_4$@TiO$_2$ magnetic adsorbent was investigated by SEM. Figure 1a shows that the TiO$_2$ is aggregated by nano-sized spherical particles after the heat-drying procedure. The pristine Fe$_3$O$_4$ with the rough surface is composed of irregular particles (Fig. 1b). As shown in Fig. 1c, the Fe$_3$O$_4$@TiO$_2$ magnetic adsorbent is present at the similar surface morphology with that of TiO$_2$, indicating that the TiO$_2$ has successfully wrapped onto

Fig. 4 Cumulative pore volume and pore size distribution of Fe$_3$O$_4$ and Fe$_3$O$_4$@TiO$_2$ magnetic adsorbent
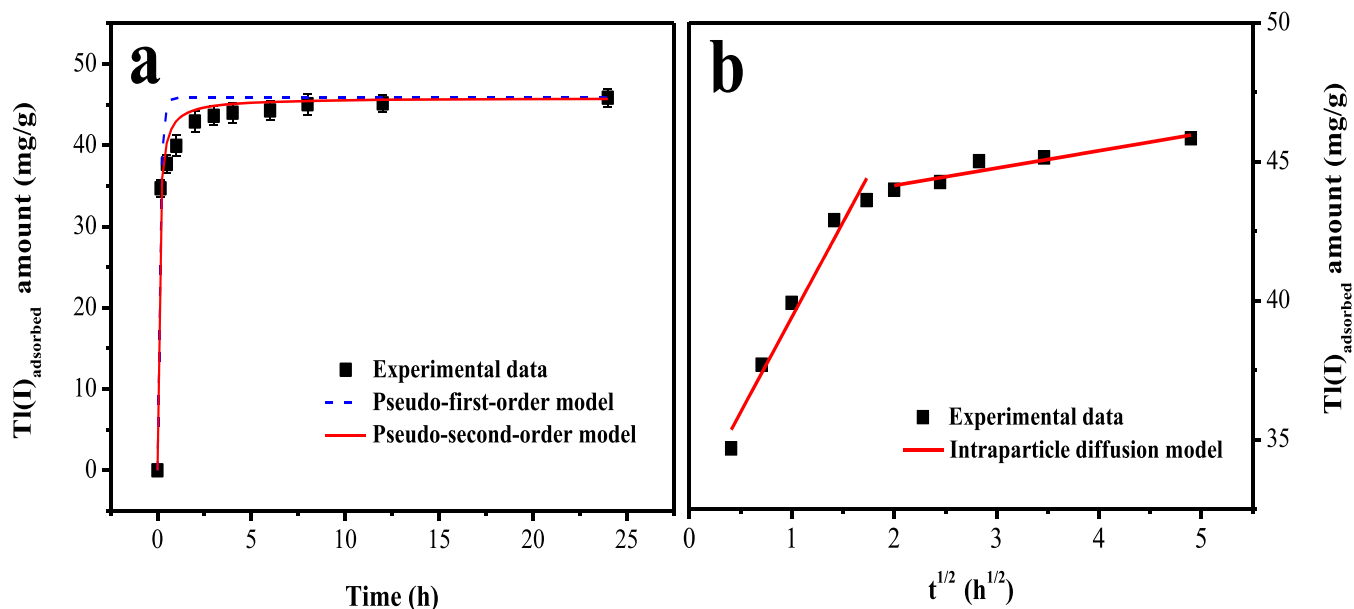
Fig. 5 Kinetics of the Tl(I) adsorption on $Fe_3O_4@TiO_2$ magnetic adsorbent: experimental data and modeling by the pseudo-first-order and pseudo-second-order models (a) and intraparticle diffusion modeling (b). $[Tl(I)]_0$ = 8 mg/L; adsorbent dosage = 0.1 g/L; pH = 7.0; T = 25 ± 1 °C

the surface of Fe_3O_4 particles during the preparation process. The increased specific surface area and a loose structure of the magnetic adsorbent due to the deposition of numerous spherical TiO_2 nanoparticles on the external surface of Fe_3O_4 particles should be beneficial for the rapid diffusion of Tl(I) towards all active sites on the adsorbent.

As shown in Fig. 2a, the particle size distribution of TiO_2, Fe_3O_4, and $Fe_3O_4@TiO_2$ magnetic adsorbent was measured using a Malvern dynamic light scattering instrument. After simple mortar grinding, TiO_2, Fe_3O_4, and $Fe_3O_4@TiO_2$ magnetic adsorbent have the mean volume diameter of 531.1, 1023.4, and 1123.6 nm, respectively. It is noted that the particle size of $Fe_3O_4@TiO_2$ magnetic adsorbent becomes slightly larger and in a narrower range, which should be attributed to the loading of TiO_2 on the surface of Fe_3O_4 particles.

Due to protonation or deprotonation of functional groups (e.g., –OH groups), the surface charge of the adsorbent can be highly affected by solution pH. It can be seen from Fig. 2b that values of isoelectric point (IEP) of TiO_2, Fe_3O_4, and $Fe_3O_4@TiO_2$ magnetic adsorbent are approximately 4.2, 6.0, and 4.8, respectively. Similar to other studies (Yin et al. 2007; Zhao et al. 2016), the IEP value of $Fe_3O_4@TiO_2$ magnetic

adsorbent turns to be obviously closer to that of TiO_2 due to the loading of TiO_2 nanoparticles. The adsorbent with a lower IEP value would have a negatively charged surface in a wider pH range, which is beneficial for its practical application in the removal of Tl(I) (will be further discussed later).

As shown in Fig. 3, several broad characteristic peaks can be observed in the XRD pattern of $Fe_3O_4@TiO_2$ magnetic adsorbent. Among them, the peaks at 30.1°, 35.6°, 57.2°, and 62.7° are assigned to characteristic peaks of Fe_3O_4 crystal particles (Yang et al. 2010), while the peaks at 25.3°, 38.1°, and 50.7° should be attributed to TiO_2 nanoparticles (PDF No. 46-1238). This further confirms that TiO_2 nanoparticles have been successfully loaded on Fe_3O_4 particles.

The BET specific surface areas of Fe_3O_4 and $Fe_3O_4@TiO_2$ magnetic adsorbent are 85.5 and 247.2 m^2/g, respectively. As seen from Fig. 4, the cumulative pore volumes of Fe_3O_4 and $Fe_3O_4@TiO_2$ magnetic adsorbent are approximately 0.30 and 0.26 cm^3/g, respectively. Notably, the pore size distribution of the $Fe_3O_4@TiO_2$ magnetic adsorbent is much narrower than that of Fe_3O_4 particles. This might be due to the coating of TiO_2 with smaller particle size on the surface of Fe_3O_4 particles.

Table 1 Kinetics parameters for the Tl(I) adsorption on $Fe_3O_4@TiO_2$ magnetic adsorbent

Pseudo-first-order			Pseudo-second-order			Intraparticle diffusion					
q_e (mg/g)	K_1 (h^{-1})	R^2	q_e (mg/g)	K_2 (g·mg^{-1}·h^{-1})	R^2	$K_{id, 1}$ (mg·g^{-1}·$h^{-1/2}$)	α_1 (mg/g)	R^2	$K_{id, 2}$ (mg·g^{-1}·$h^{-1/2}$)	α_2 (mg/g)	R^2
45.84	7.79	0.94	45.84	0.325	0.99	6.84	32.6	0.95	0.625	42.9	0.88

Fig. 6 Effect of solution pH on the Tl(I) adsorption by $Fe_3O_4@TiO_2$ magnetic adsorbent. $[Tl(I)]_0 = 8$ mg/L; adsorbent dosage = 0.1 g/L; T = 25 ± 1 °C
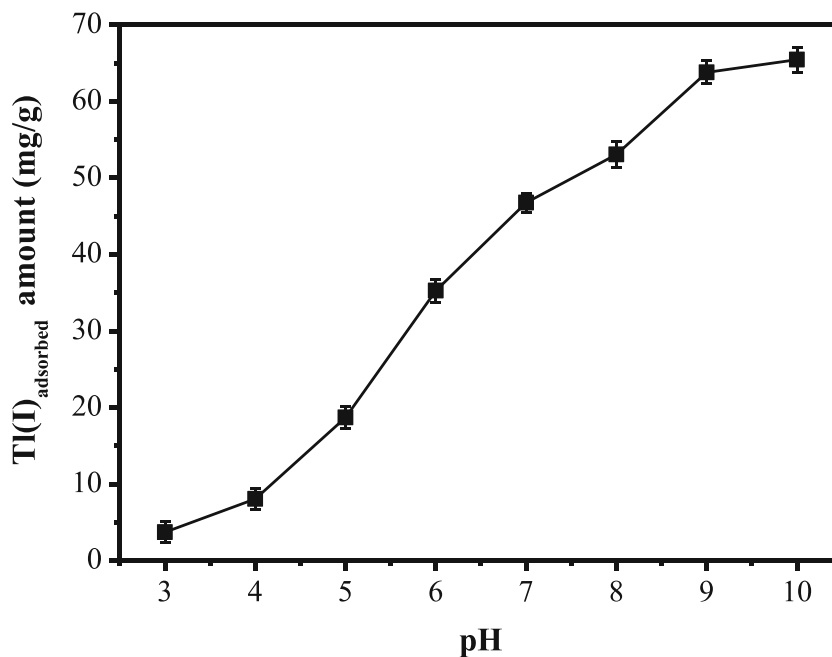
Kinetics study

The adsorption kinetics study is of crucial importance to evaluate the adsorption performance of the $Fe_3O_4@TiO_2$ magnetic adsorbent. Figure 5a demonstrates that approximately 82% of maximum Tl(I) loading amount can rapidly occur in the first 0.5 h, followed by a relatively slow adsorption process and the equilibrium can be reached within 12 h.

In order to better understand the adsorption kinetics of Tl(I) on the adsorbent, the pseudo-first-order, pseudo-second-order, and intraparticle diffusion models were employed for simulating the experimental data. The mathematical equations of these theoretical kinetics models are given as follows:

$$q_t = q_e\left(1 - e^{-K_1 t}\right) \tag{3}$$

$$q_t = \frac{q_e^2 K_2 t}{1 + K_2 q_e t} \tag{4}$$

$$q_t = K_{id} t^{1/2} + \alpha \tag{5}$$

Fig. 7 Adsorption isotherm of Tl(I) on $Fe_3O_4@TiO_2$ magnetic adsorbent at pH 7.0. Adsorbent dosage = 0.1 g/L; T = 25 ± 1 °C
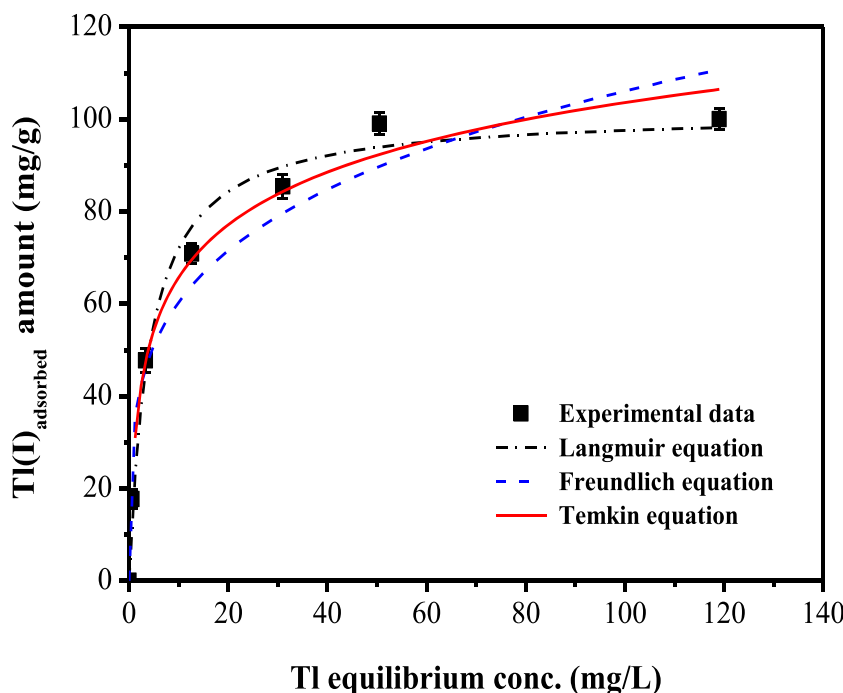
Table 2 Langmuir, Freundlich, and Temkin isotherm parameters for the Tl(I) adsorption

Langmuir isotherm			Freundlich isotherm			Temkin isotherm		
q_{max} (mg/g)	K_L (L/mg)	R^2	K_f (mg$^{(1-1/n)}$L$^{1/n}$/g)	$1/n$	R^2	A (L/g)	b (kJ/mol)	R^2
101.5	0.244	0.99	34.38	0.245	0.96	5.50	0.151	0.99

where q_e and q_t (mg/g) are the adsorption amount of Tl(I) on the adsorbent at equilibrium and time t (h), respectively; K_1 (h^{-1}), K_2 (g·mg^{-1}·h^{-1}), and K_{id} (mg·g^{-1}·h$^{-1/2}$) are the rate constant of the pseudo-first-order, pseudo-second-order, and intraparticle diffusion models, respectively; α (mg/g) refers to the boundary layer effect.

The constants and correlation coefficients (R^2) obtained from kinetics models are summarized in Table 1. According to the values of R^2, the pseudo-second-order model seems to be more suitable for fitting the experimental data than the pseudo-first-order model. The pseudo-second-order model assumes that the rate-limiting step of the adsorption process is controlled by chemical reactions in which adsorbed ions are bonded onto the adsorbent surface by strong covalent bonding (Inglezakis et al. 2019). Therefore, the adsorption of Tl(I) on the Fe$_3$O$_4$@TiO$_2$ magnetic adsorbent could be a chemisorption process.

The adsorption process can be divided into three steps including the external diffusion from the bulk solution to the exterior surface of the adsorbent, the diffusion into the interior pores of the adsorbent (namely intraparticle diffusion), and the final adsorption on the active sites of the adsorbent. Since the adsorption of Tl(I) on the adsorbent is governed by a chemisorption process, the third step should be very rapid and the adsorption rate might be controlled by external or intraparticle diffusion process. As shown in Fig. 5b, the intraparticle diffusion modeling shows a multilinearity. The first linear stage

with a higher rate constant suggests that the adsorption is dominated by the intraparticle diffusion, while the second linear stage refers to the equilibrium process of which rate constant is far lower than the first stage owing to a dramatic reduction of the Tl(I) concentration in solution. As illustrated in Table 1, the value of α_1 equals to 32.6 mg/g that is attributed to the effect of boundary layer. It is worthwhile to note that this portion of the Tl(I) loading amount can be achieved within 10 min, indicating that over 71% of active sites are present on the external surface of the adsorbent. The adsorption rate of Tl(I) would be therefore limited by both the external diffusion and intraparticle diffusion.

pH effect

As shown in Fig. 6, the loading amount of Tl(I) on the adsorbent increases with an increase in solution pH and the optimal adsorption is achieved at pH 10.0. This is consistent with the results reported in other studies that the adsorption of Tl(I) on titanium-based adsorbents could be highly affected by the electrostatic interaction between adsorbents and Tl(I) ions (Zhang et al. 2018). In brief, the dominant species of Tl(I) ions in the tested pH range of 4.0–10.0 are in the form of Tl$^+$ ions. The adsorbent surface could be positively charged at pH below the IEP value (4.8 for Fe$_3$O$_4$@TiO$_2$ magnetic adsorbent), leading to strong electrostatic repulsion between Tl$^+$ ions and the adsorbent. As a result, the uptake of Tl(I) is

Table 3 Adsorption capacities of Tl(I) on previously reported adsorbents

Adsorbent	Tl(I) conc. range (mg/L)	pH	Max. adsorption capacity (mg/g)	Reference
Treated sawdust	0–1000	7.0	13.18	(Memon et al. 2008)
Multiwalled carbon nanotube	0–0.12	6.0	0.42	(Pu et al. 2013)
FeOOH-loaded MnO$_2$	10–150	7.0	450	(Chen et al. 2017)
Titanium peroxide	5–130	7.0	412	(Zhang et al. 2018)
Titanium dioxide	5–130	7.0	258	(Zhang et al. 2018)
Titanate nanotube	0–60	5.0	709.2	(Liu et al. 2014)
MnO$_2$@pyrite cinder	0–160	12.0	320	(Li et al. 2018)
Titanate nanomaterials	25–600	8.0	710.4	(Wang et al. 2020)
Thiol-functionalized mesoporous silica submicrospheres	10–300	6.0	452.8	(Soltani et al. 2019)
Wire-like MnO$_2$	5–1000	6.0	450	(Li et al. 2019)
Fe$_3$O$_4$@TiO$_2$	5–150	7.0	101.5	This study

Fig. 8 Effect of co-existing cations on the Tl(I) adsorption by $Fe_3O_4@TiO_2$ magnetic adsorbent. $[Tl(I)]_0 = 8$ mg/L; adsorbent dosage = 0.1 g/L; T = 25 ± 1 °C; pH = 5.0
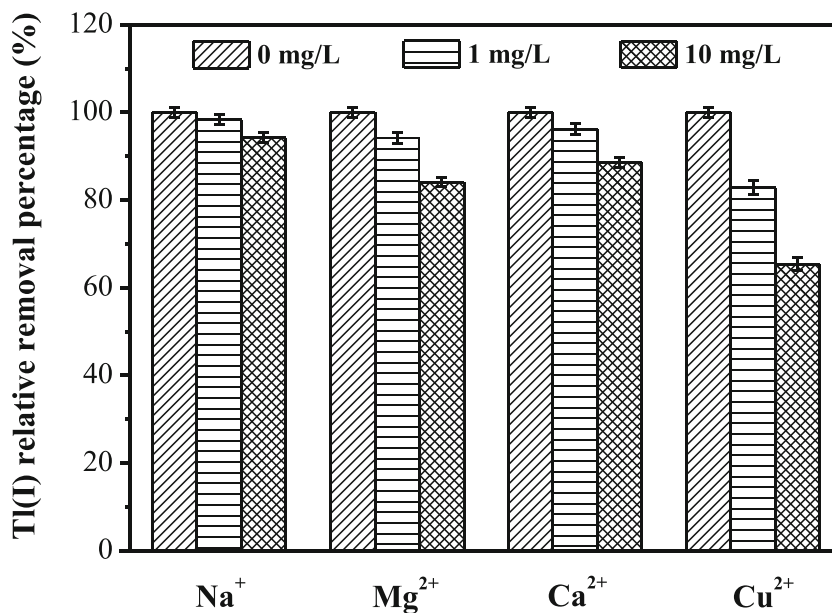
retarded. The adsorbent surface charge will turn to be negative at pH above the IEP value. The enhanced electrostatic attraction between the adsorbent and Tl(I) would be favorable for the adsorption process, resulting in the increased uptake of Tl(I) with increasing solution pH.

Adsorption isotherm

The adsorption isotherm experiment was conducted at pH 7.0 and the results are shown in Fig. 7. In order to better understand the adsorption process, the Langmuir, Freundlich, and Temkin equations were employed for fitting the experimental data. The Langmuir, Freundlich, and Temkin equations are expressed as follows (Karri et al. 2017):

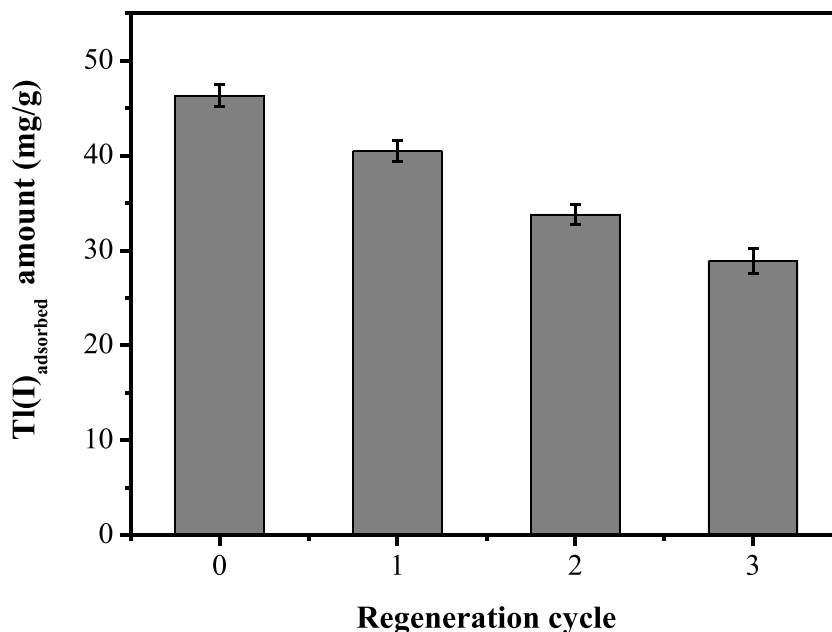$$q_e = \frac{q_{max}K_L C_e}{1 + K_L C_e} \tag{6}$$

$$q_e = K_f C_e^{1/n} \tag{7}$$

$$q_e = \left(\frac{RT}{b}\right) ln(AC_e) \tag{8}$$

where q_e and C_e are the adsorbed amount of Tl(I) at equilibrium (mg/g) and the equilibrium concentration of Tl(I) in

Fig. 9 Regeneration performance of $Fe_3O_4@TiO_2$ magnetic adsorbent. $[Tl(I)]_0 = 8$ mg/L; adsorbent dosage = 0.1 g/L; T = 25 ± 1 °C; pH = 7.0

solution (mg/L), respectively. q_{max} is the maximum adsorption capacity (mg/g), K_L is the Langmuir coefficient relating to the adsorption strength (L/mg), K_f is the constant for relative adsorption capacity ($mg^{(1-1/n)}L^{1/n}/g$), and n is the affinity constant. A is the Temkin isotherm constant (L/g), b is the constant relating to the heat of adsorption (kJ/mol), R is the universal gas constant (8.314×10^3 kJ/mol·K), and T is the absolute temperature (K).

The parameters and correlation coefficient (R^2) obtained from isotherm models are listed in Table 2. According to the value of R^2, both the Langmuir and Temkin equations can work well on the fitting of experimental data. The maximum adsorption capacity of the adsorbent is calculated as 101.5 mg/g at pH 7.0, suggesting that the prepared magnetic adsorbent is a competitive substitute for the effective removal of Tl(I) from water compared to other previously reported adsorbents as illustrated in Table 3. The value of b obtained from the Temkin model is 0.151 kJ/mol, indicating that the uptake of Tl(I) on the adsorbent also involves the physisorption process to some extent (Zhang et al. 2018).

Selectivity and regeneration study

Since the cations such as Na^+, Mg^{2+}, Ca^{2+}, and Cu^{2+} widely exist in natural waters and industrial wastewaters, their presence can compete for active sites on the adsorbent with Tl(I) ions. As shown in Fig. 8, the influence of these co-existing cations in the removal percentage of Tl(I) follows the order: $Cu^{2+} > Mg^{2+} > Ca^{2+} > Na^+$. The reduction in the Tl(I) uptake

by approximately 35% is observed when the Cu^{2+} concentration is as high as 10 mg/L.

The obviously negative effect on the Tl(I) uptake at the presence of these co-existing cations might be due to their similar nature of chemistry with Tl(I) ions (e.g., ionic radius and electronegativity) (Depci et al. 2012). Therefore, they can exhibit a strong competition with Tl(I) for active sites on the adsorbent.

As shown in Fig. 9, the $Fe_3O_4@TiO_2$ magnetic adsorbent can be effectively regenerated by 0.1 M HNO_3 solution. The Tl(I) loading amount in cycle 0 refers to that of the virgin adsorbent. After the first- and third-regeneration cycles, the Tl(I) loading amount of the adsorbent can be recovered as 40.48 and 28.91 mg/g, respectively.

Mechanism study

As seen in Fig. 10, the main characteristic peaks of Ti, C, and O can be observed on the XPS wide-scan spectra of both the virgin and Tl-loaded adsorbents. Only a weak peak assigned to Fe 2p is detected, indicating that Fe_3O_4 particles have been fully coated by TiO_2 nanoparticles. A new peak attributed to Tl 4f appears on the XPS spectrum of the Tl-loaded adsorbent, which confirms the adsorption of Tl(I) on the adsorbent.

Ti 2p, Tl 4f, and O 1s high-resolution XPS spectra of adsorbents before and after the adsorption are shown in Fig. 11. The Ti 2p spectrum for titanium element is composed of two asymmetric peaks, namely Ti 2p3/2 and Ti 2p1/2 (Fig. 11a). The binding energy of the Ti 2p3/2 peak in the virgin

Fig. 10 XPS wide-scan spectra of adsorbents before and after the Tl(I) adsorption
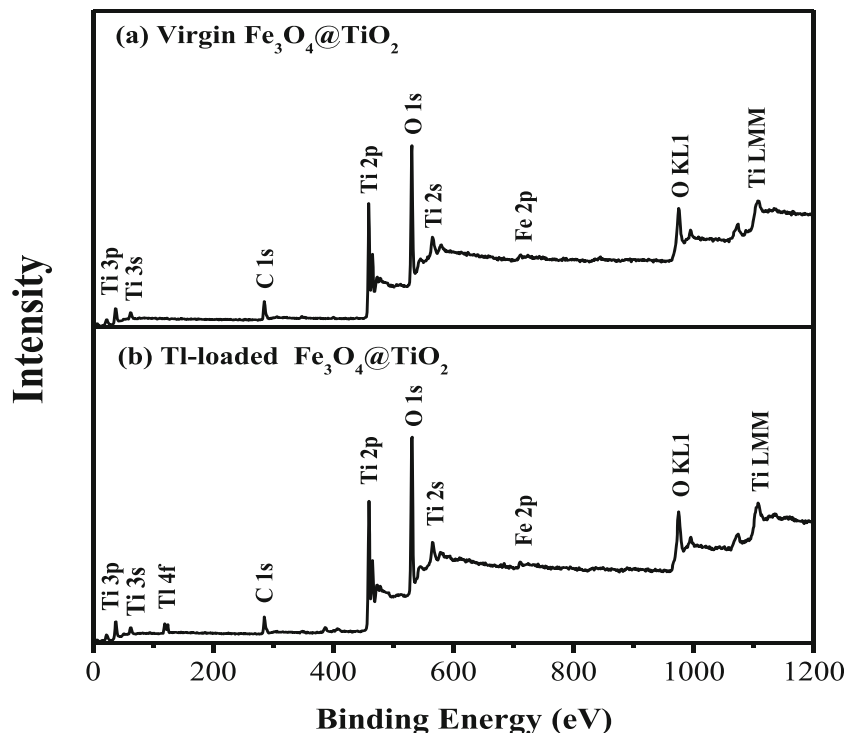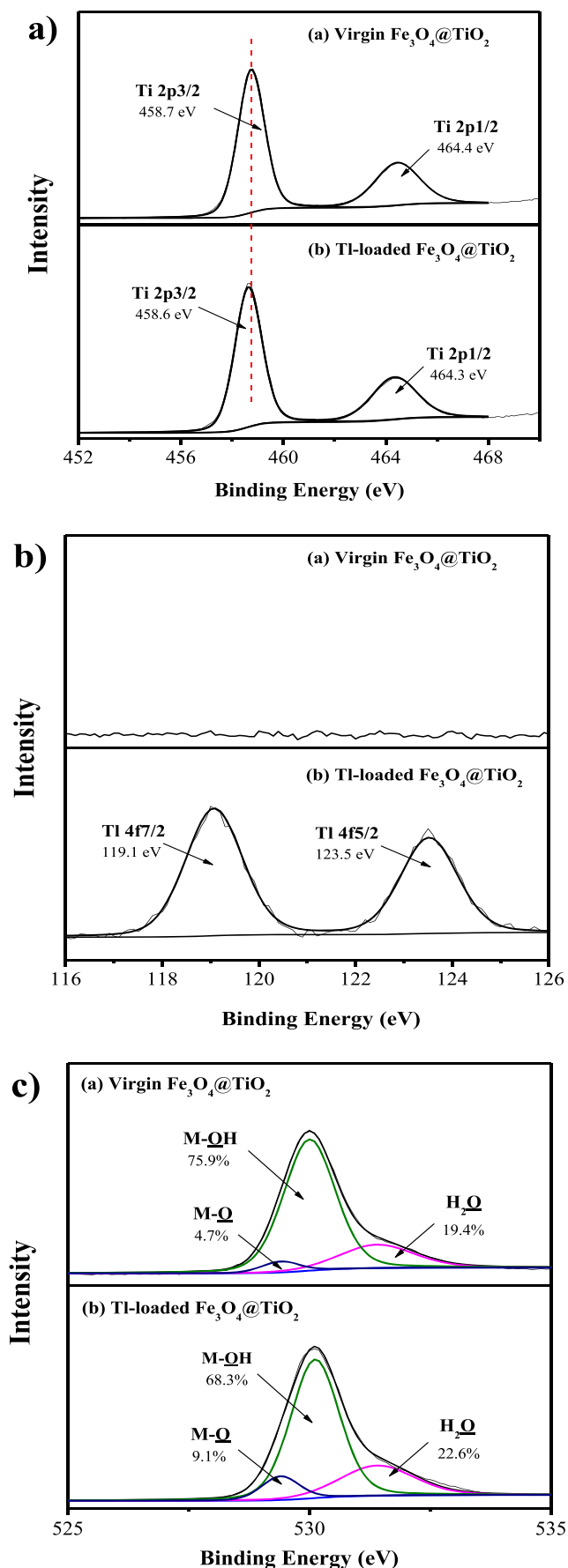
◀ **Fig. 11** Ti 2p (**a**), Tl 4f (**b**), and O 1s (**c**) high-resolution XPS spectra of adsorbents before and after the Tl(I) adsorption

adsorbent is determined as 458.7 eV, suggesting that the valence state of titanium element is +V. It is clearly seen that the Ti 2p3/2 peak slightly shifts to a lower binding energy position after the adsorption, which might be caused by the binding of electropositive Tl(I) ions.

As shown in Fig. 11b, the characteristic peak of thallium on the Tl-loaded adsorbent has two asymmetric component peaks at 119.1 and 123.5 eV which are assigned to Tl 4f7/2 and Tl 4f5/2, respectively. This indicates that the oxidation state of adsorbed thallium is not changed and there is no redox reaction occurred on the adsorbent surface (Wan et al. 2014; Zhang et al. 2018).

The O 1s high-resolution XPS spectra of the virgin and Tl-loaded adsorbents were further analyzed for better understanding of the adsorption mechanism. As shown in Fig. 11c, the O 1s spectra can be decomposed into three component peaks. The peaks at the binding energies of 529.4, 530.1, and 531.4 eV are attributed to M–O, M–OH, and adsorbed H_2O, respectively. After the Tl(I) adsorption, the content of M–OH decreases from 75.9 to 68.3%, while the contents of M–O and adsorbed H_2O increase from 4.7 to 9.1% and 19.4 to 22.6%, respectively. This suggests that hydroxyl groups bonded on Ti atoms may play a key role in the adsorption process.

According to the change of relative contents of functional groups and results from batch experiments, the hydroxyl groups on the adsorbent surface should greatly participate into the adsorption process. The electrostatic interaction between the adsorbent and Tl(I) ions may significantly affect the Tl(I) uptake. During the adsorption, Tl(I) ions can be rapidly and effectively adsorbed on the adsorbent surface through the formation of the linkages of Ti–O–Tl.

Conclusions

In this study, the $Fe_3O_4@TiO_2$ core-shell magnetic adsorbent was successfully synthesized for the effective removal of Tl(I) ions from water. SEM images showed that Fe_3O_4 particles could be fully wrapped by nano-sized spherical TiO_2 particles, leading to an obvious reduction in the isoelectric point of the adsorbent and nearly threefold higher BET specific surface area than pristine Fe_3O_4 particles. The adsorption of Tl(I) on the adsorbent was found to be pH-dependent. The maximum adsorption capacity of the adsorbent at pH 7.0 was determined as 101.5 mg/g according to the Langmuir isotherm model. The existence of co-existing cations could have some negative effect on the uptake of Tl(I). The Tl(I) ions were adsorbed on the adsorbent surface through the formation of Ti–O–Tl

linkages and there was no redox reaction occurred during the adsorption. The prepared magnetic adsorbent could be considered as a promising substitute for the effective removal of Tl(I) from water owing to its high adsorption capacity and facile recoverability under external magnetic field.

References

Alijani H, Shariatinia Z, Aroujalian Mashhadi A (2015) Water assisted synthesis of MWCNTs over natural magnetic rock: an effective magnetic adsorbent with enhanced mercury(II) adsorption property. Chem Eng J 281:468–481

Chen M, Wu P, Yu L, Liu S, Ruan B, Hu H, Zhu N, Lin Z (2017) FeOOH-loaded MnO$_2$ nano-composite: an efficient emergency material for thallium pollution incident. J Environ Manage 192:31–38

Davies M, Figueroa L, Wildeman T, Bucknam C (2016) The oxidative precipitation of thallium at alkaline pH for treatment of mining influenced water. Mine Water Environ 35:77–85

Depci T, Kul A, Önal Y (2012) Competitive adsorption of lead and zinc from aqueous solution on activated carbon prepared from Van apple pulp: Study in single- and multi-solute systems. Chem Eng J 200-202:224–236

Galván-Arzate S, SantamaríA A (1998) Thallium toxicity. Toxicol Lett 99: 1-13

Huangfu X, Jin J, Lu X, Wang Y, Liu Y, Pang S, Cheng H, Xiang Z, Ma J (2015) Adsorption and oxidation of thallium(I) by a nanosized manganese dioxide. Water Air Soil Pollut 226:2272

Inglezakis V, Fyrillas M, Park J (2019) Variable diffusivity homogeneous surface diffusion model and analysis of merits and fallacies of simplified adsorption kinetics equations. J Hazard Mater 367:224–245

Kajitvichyanukul P, Chenthamarakshan C, Rajeshwar K, Qasim S (2003) Adsorption of thallium(I) ions on titania particle surfaces in aqueous media. Adsorpt Sci Technol 21:217–228

Karri R, Sahu J, Jayakumar N (2017) Optimal isotherm parameters for phenol adsorption from aqueous solutions onto coconut shell based activated carbon: error analysis of linear and non-linear methods. J Taiwan Inst Chem Eng 80:472–487

Khavidaki H, Aghaie H (2013) Adsorption of thallium(I) ions using eucalyptus leaves powder. Clean Soil Air Water 41:673–679

Koduru J, Karri R, Mubarak N (2019) Smart materials, magnetic graphene oxide-based nanocomposites for sustainable water purification. In: Thomas S, Kumar Mishra R, Asiri AM (eds) Inamuddin. Sustainable Polymer Composites and Nanocomposites. Springer International Publishing, Cham, pp 759–781

Li H, Chen Y, Long J, Jiang D, Liu J, Li S, Qi J, Zhang P, Wang J, Gong J (2017) Simultaneous removal of thallium and chloride from a highly saline industrial wastewater using modified anion exchange resins. J Hazard Mater 333:179–185

Li H, Li X, Xiao T, Chen Y, Long J, Zhang G, Zhang P, Li C, Zhuang L, Li K (2018) Efficient removal of thallium(I) from wastewater using flower-like manganese dioxide coated magnetic pyrite cinder. Chem Eng J 353:867–877

Li K, Li H, Xiao T, Long J, Zhang G, Li Y, Liu X, Liang Z, Zheng F, Zhang P (2019) Synthesis of manganese dioxide with different morphologies for thallium removal from wastewater. J Environ Manage 251:109563

Lingamdinne L, Koduru J, Chang Y, Karri R (2018) Process optimization and adsorption modeling of Pb(II) on nickel ferrite-reduced graphene oxide nano-composite. J Mol Liq 250:202–211

Lingamdinne L, Koduru J, Karri R (2019) A comprehensive review of applications of magnetic graphene oxide based nanocomposites for sustainable water purification. J Environ Manage 231:622–634

Liu W, Zhang P, Borthwick A, Chen H, Ni J (2014) Adsorption mechanisms of thallium(I) and thallium(III) by titanate nanotubes: ion-exchange and co-precipitation. J Colloid Interface Sci 423:67–75

Memon S, Memon N, Solangi A, Memon J (2008) Sawdust: a green and economical sorbent for thallium removal. Chem Eng J 140:235–240

Mulkey J, Oehme F (1993) A review of thallium toxicity. Vet Hum Toxicol 35:445–453

Peter A, Viraraghavan T (2008) Removal of thallium from aqueous solutions by modified Aspergillus niger biomass. Bioresour Technol 99:618–625

Pu Y, Yang X, Hong Z, Wang D, Yu S, Jie H (2013) Adsorption and desorption of thallium(I) on multiwalled carbon nanotubes. Chem Eng J 219:403–410

Rasoulzadeh H, Dehghani M, Mohammadi A, Karri R, Nabizadeh R, Nazmara S, Kim K, Sahu J (2020) Parametric modelling of Pb(II) adsorption onto chitosan-coated Fe$_3$O$_4$ particles through RSM and DE hybrid evolutionary optimization framework. J Mol Liq 297: 111893

Rehman S, Ullah N, Kamali A, Ali K, Yerlikaya C, Rehman H (2013) Study of thallium(III) adsorption onto multiwall carbon nanotubes. Carbon 55:375

Ruthiraan M, Mubarak N, Abdullah E, Khalid M, Nizamuddin S, Walvekar R, Karri R (2019) An overview of magnetic material: preparation and adsorption removal of heavy metals from wastewater. In: Abd-Elsalam KA, Mohamed MA, Prasad R (eds) Magnetic Nanostructures : Environmental and Agricultural Applications. Springer International Publishing, Cham, pp 131–159

Sabermahani F, Mahani N, Noraldiny M (2017) Removal of thallium (I) by activated carbon prepared from apricot nucleus shell and modified with rhodamine B. J Toxicol Toxin Rev 36:154–160

Soltani R, Marjani A, Shirazian S (2019) Facile one-pot synthesis of thiol-functionalized mesoporous silica submicrospheres for Tl(I) adsorption: Isotherm, kinetic and thermodynamic studies. J Hazard Mater 371:146–155

Wan S, Ma M, Lv L, Qian L, Xu S, Xue Y, Ma Z (2014) Selective capture of thallium(I) ion from aqueous solutions by amorphous hydrous manganese dioxide. Chem Eng J 239:200–206

Wang N, Su Z, Deng N, Qiu Y, Ma L, Wang J, Chen Y, Hu K, Huang C, Xiao T (2020) Removal of thallium(I) from aqueous solutions using titanate nanomaterials: the performance and the influence of morphology. Sci Total Environ 717:137090

Yang L, Xiao J, Shen Y, Liu X, Li W, Wang W, Yang Y (2017) The efficient removal of thallium from sintering flue gas desulfurization wastewater in ferrous metallurgy using emulsion liquid membrane. Environ Sci Pollut Res 24:24214–24222

Yang Z, Gong X, Zhang C (2010) Recyclable Fe$_3$O$_4$/hydroxyapatite composite nanoparticles for photocatalytic applications. Chem Eng J 165:117–121

Yin CY, Aroua MK, Daud WMAW (2007) Impregnation of palm shell activated carbon with polyethyleneimine and its effects on Cd^{2+} adsorption. Colloids Surf A 307:128–136

Yin H, Kong M, Gu X, Chen H (2017) Removal of arsenic from water by porous charred granulated attapulgite-supported hydrated iron oxide in bath and column modes. J Cleaner Prod 166:88–97

Yu Y, Yu L, Shih K, Chen J (2018) Yttrium-doped iron oxide magnetic adsorbent for enhancement in arsenic removal and ease in separation after applications. J Colloid Interface Sci 521:252–260

Zhang G, Fang F, Li X, Qi J, Chen Y (2018) Superior adsorption of thallium(I) on titanium peroxide: performance and mechanism. Chem Eng J 331:471–479

Zhang H, Chen D, Cai S, Tu G, Luo D, Chen Y (2013) Research on treating thallium by enhanced coagulation oxidation process. Agric Sci Technol 14:1322–1324

Zhang L, Huang T, Zhang M, Guo X, Yuan Z (2008) Studies on the capability and behavior of adsorption of thallium on nano-Al_2O_3. J Hazard Mater 157:352–357

Zhao D, Yang Y, Chen J (2016) Fabrication and testing of zirconium-based nano-particle doped activated carbon fiber for enhanced arsenic removal in water. RSC Adv 6:27020–27030

Publisher's note Springer Nature remains neutral with regard to jurisdictional claims in published maps and institutional affiliations.